

---

# Quaternion Recurrent Neural Networks

---

**Titouan Parcollet**<sup>1,4</sup>   **Mirco Ravanelli**<sup>2</sup>   **Mohamed Mochid**<sup>1</sup>  
**Georges Linarès**<sup>1</sup>   **Chiheb Trabelsi**<sup>2</sup>   **Renato De Mori**<sup>1,3</sup>   **Yoshua Bengio**<sup>2\*</sup>

<sup>1</sup>LIA, Université d’Avignon, France

<sup>2</sup>MILA, Université de Montréal, Québec, Canada

<sup>3</sup>McGill University, Québec, Canada

<sup>4</sup>Orkis, Aix-en-provence, France

[titouan.parcollet@alumni.univ-avignon.fr](mailto:titouan.parcollet@alumni.univ-avignon.fr)

[mirco.ravanelli@gmail.com](mailto:mirco.ravanelli@gmail.com)

[firstname.lastname@univ-avignon.fr](mailto:firstname.lastname@univ-avignon.fr)

[chiheb.trabelsi@polymtl.ca](mailto:chiheb.trabelsi@polymtl.ca)   [rdemori@cs.mcgill.ca](mailto:rdemori@cs.mcgill.ca)

## Abstract

Recurrent neural networks (RNNs) are powerful architectures to model sequential data, due to their capability to learn short and long-term dependencies between the basic elements of a sequence. Nonetheless, popular tasks such as speech or images recognition, involve multi-dimensional input features that are characterized by strong internal dependencies between the dimensions of the input vector. We propose a novel quaternion recurrent neural network (QRNN) that takes into account both the external relations and these internal structural dependencies with the quaternion algebra. Similarly to capsules, quaternions allow the QRNN to code internal dependencies by composing and processing multidimensional features as single entities, while the recurrent operation reveals correlations between the elements composing the sequence. We show that the QRNN achieves better performances in both a synthetic memory copy task and in realistic applications of automatic speech recognition. Finally, we show that the QRNN reduces by a factor of 3x the number of free parameters needed, compared to RNNs to reach better results, leading to a more compact representation of the relevant information.

## 1 Introduction and motivations

In the last few years, deep neural networks (DNN) have encountered a wide success in different domains due to their capability to learn highly complex input to output mapping. Among the different DNN-based models, the recurrent neural network (RNN) is well adapted to represent sequential data. Indeed, RNNs build a vector of activations at each timestep to code latent relations between input vectors. However, many recent tasks based on multi-dimensional input features, such as pixels of an image, acoustic features, or 3D models, require to represent both external dependencies between each entity, and internal relations between the features that compose this entity. Furthermore, the relations between two distant elements in a long sequence of input features are difficult to catch due to the vanishing gradient problem [4, 24], making it hard to capture both external and internal dependencies in the same manner.

Quaternions are hypercomplex numbers that contain a real and three separate imaginary components, fitting perfectly to 3 and 4 dimensional feature vectors, such as for image processing and robot kinematics [3, 25, 29]. The idea of bundling groups of numbers into separate entities is also

---

\*CIFAR Senior Fellow

exploited by the recent capsule network [28]. Contrary to traditional homogeneous representations, capsule and quaternion networks bundle sets of features together. Thereby, quaternion numbers allow neural network based models to code latent inter-dependencies between groups of input features during the learning process with less parameters than RNNs, by taking advantage of the *Hamilton product* as the equivalent of the ordinary product, but between quaternions. In the proposed architecture, the features of the input vector are linked in the latent space of quaternions with a single quaternion weight devoted to memorize these relations. This is how we achieve considerably reduced numbers of parameters than other RNNs: a 4-number quaternion weight linking two 4-number quaternion units only has 4 degrees of freedom, whereas a standard neural net parametrization would have  $4 \times 4 = 16$ , i.e., a 4-fold saving in memory, computation and degrees of freedom. Early applications of quaternions-valued backpropagation algorithms [1, 2] have efficiently solved quaternion functions approximation tasks. More recently, neural networks of complex and hypercomplex numbers have received an increasing attention with motivations described in [7, 13, 35, 36], and some efforts have shown promising results in different applications. In particular, a deep quaternion network [22, 23, 33], a deep quaternion convolutional network [5], or a deep complex convolutional network [34] have been successfully employed for challenging tasks such as images and language processing. However, none of these applications merged recurrent neural networks and the quaternion algebra. This paper proposes a novel model called quaternion recurrent neural network<sup>2</sup> (QRNN), with a well-adapted parameters initialization, for learning both inter- and intra-dependencies between multidimensional input features and the basic elements of a sequence (Section 2).

The effectiveness of the proposed QRNN is first evaluated on a memory copy task [14] (Section 3.1) to highlight the ability of QRNNs to learn long and short term dependencies. The experimental validation is then extended to more realistic automatic speech recognition tasks (Section 3.2), with the standard TIMIT phoneme recognition and the Wall Street Journal (WSJ) task. Indeed, modern automatic speech recognition systems usually employ input sequences composed of multidimensional acoustic features, such as mel filter banks, that are often enriched with their first, second and third time derivatives [8, 9], to integrate contextual information. In standard RNNs, static features are simply concatenated with their derivatives to form a large input vector, without effectively considering that signal derivatives represent different views of the same input. We hypothesize that for such data, quaternion RNNs naturally provide a more suitable representation of the input sequence, since these multiple views can be directly embedded in the multiple dimensions space of the quaternion. The conducted experiments show that the QRNN successfully solves the short and long term dependencies challenge on the memory copy task. QRNNs also obtain better performances than RNNs on the TIMIT phoneme recognition task with a phoneme error rate (PER) of 17.0% compared to 17.3% for RNNs, while requiring considerably fewer parameters. Indeed, the QRNN reaches these promising performances with up to 3 times less learning parameters than the RNN. We also show that the QRNN obtains a lower PER than the RNN with an equivalent number of free parameters. These statements are extended to the WSJ corpus with better word error rate (WER) for the QRNN compared to real-valued RNNs, with 2.55x less free parameters for the QRNN.

## 2 Quaternion recurrent neural networks

This section describes the quaternion algebra, the internal quaternion representation, the backpropagation through time (BPTT) applied to the quaternion domain, and proposes an adapted weight initialization to quaternion-valued neurons.

### 2.1 Quaternion algebra

The quaternion algebra  $\mathbb{H}$  defines operations between quaternion numbers. A quaternion  $Q$  is an extension of a complex number defined in a four dimensional space as:

$$Q = r\mathbf{1} + x\mathbf{i} + y\mathbf{j} + z\mathbf{k}, \quad (1)$$

where  $r$ ,  $x$ ,  $y$ , and  $z$  are real numbers, and  $\mathbf{1}$ ,  $\mathbf{i}$ ,  $\mathbf{j}$ , and  $\mathbf{k}$  are the quaternion unit basis. In a quaternion,  $r$  is the real part, while  $x\mathbf{i} + y\mathbf{j} + z\mathbf{k}$  with  $\mathbf{i}^2 = \mathbf{j}^2 = \mathbf{k}^2 = \mathbf{ijk} = -1$  is the imaginary part, or the

---

<sup>2</sup>The full code for QRNNs is available at <https://github.com/TParcollet/Quaternion-Recurrent-Neural-Networks>

vector part. Such a definition can be used to describe spatial rotations. The information embedded in the quaternion  $Q$  can be summarized into the following matrix of real numbers, that turns out to be more suitable for computations:

$$Q_{mat} = \begin{bmatrix} r & -x & -y & -z \\ x & r & -z & y \\ y & z & r & -x \\ z & -y & x & r \end{bmatrix}. \quad (2)$$

The conjugate  $Q^*$  of  $Q$  is defined as:

$$Q^* = r\mathbf{1} - x\mathbf{i} - y\mathbf{j} - z\mathbf{k}. \quad (3)$$

Then, a normalized or unit quaternion  $Q^\triangleleft$  is expressed as:

$$Q^\triangleleft = \frac{Q}{\sqrt{r^2 + x^2 + y^2 + z^2}}. \quad (4)$$

Finally, the Hamilton product  $\otimes$  between two quaternions  $Q_1$  and  $Q_2$  is computed as follows:

$$\begin{aligned} Q_1 \otimes Q_2 = & (r_1 r_2 - x_1 x_2 - y_1 y_2 - z_1 z_2) + \\ & (r_1 x_2 + x_1 r_2 + y_1 z_2 - z_1 y_2) \mathbf{i} + \\ & (r_1 y_2 - x_1 z_2 + y_1 r_2 + z_1 x_2) \mathbf{j} + \\ & (r_1 z_2 + x_1 y_2 - y_1 x_2 + z_1 r_2) \mathbf{k}. \end{aligned} \quad (5)$$

The Hamilton product is used in QRNNs to perform transformations of vectors representing quaternions, as well as scaling and interpolation between two rotations following a geodesic over a sphere in the  $\mathbb{R}^3$  space as shown in [18].

## 2.2 Quaternion representation

The QRNN is an extension of the real-valued [17] and complex-valued [15, 30] recurrent neural networks to hypercomplex numbers. In a quaternion dense layer, all parameters are quaternions, including inputs, outputs, weights, and biases. The quaternion algebra is ensured by manipulating matrices of real numbers [5]. Consequently, for each input vector of size  $N$ , output vector of size  $M$ , dimensions are split into four parts: the first one equals to  $r$ , the second is  $x\mathbf{i}$ , the third one equals to  $y\mathbf{j}$ , and the last one to  $z\mathbf{k}$  to compose a quaternion  $Q = r\mathbf{1} + x\mathbf{i} + y\mathbf{j} + z\mathbf{k}$ . The inference process of a fully-connected layer is defined in the real-valued space by the dot product between an input vector and a real-valued  $M \times N$  weight matrix. In a QRNN, this operation is replaced with the Hamilton product (eq. 5) with quaternion-valued matrices (i.e. each entry in the weight matrix is a quaternion).

## 2.3 Learning algorithm

The QRNN differs from the real-valued RNN in each learning sub-processes. Therefore, let  $x_t$  be the input vector at timestep  $t$ ,  $h_t$  the hidden state,  $W_{hx}$ ,  $W_{hy}$  and  $W_{hh}$  the input, output and hidden states weight matrices respectively. The vector  $b_h$  is the bias of the hidden state and  $p_t$ ,  $y_t$  are the output and the expected target vectors.

### 2.3.1 Forward phase

Based on the forward propagation of the real-valued RNN [17], the QRNN forward equations are extended as follows:

$$h_t = \alpha(W_{hh} \otimes h_{t-1} + W_{hx} \otimes x_t + b_h), \quad (6)$$

where  $\alpha$  is a *quaternion split activation function* [37] defined as:

$$\alpha(Q) = f(r) + f(x)\mathbf{i} + f(y)\mathbf{j} + f(z)\mathbf{k}, \quad (7)$$

with  $f$  corresponding to any standard activation function. The output vector  $p_t$  is computed as:

$$p_t = \beta(W_{hy} \otimes h_t), \quad (8)$$

where  $\beta$  is any split activation function. Finally, the objective function is a classical real-valued loss applied component-wise (e.g., mean squared error, negative log-likelihood).

### 2.3.2 Quaternion Backpropagation Through Time

The backpropagation through time (BPTT) for quaternion numbers is an extension of the standard quaternion backpropagation [21], and its full derivation is available in Appendix 5.2. The gradient with respect to the loss  $E_t$  is expressed for each weight matrix as  $\Delta_{hy} = \frac{\partial E_t}{\partial W_{hy}}$ ,  $\Delta_{hh} = \frac{\partial E_t}{\partial W_{hh}}$ , and  $\Delta_{hx} = \frac{\partial E_t}{\partial W_{hx}}$ , and can be generalized to  $\Delta = \frac{\partial E_t}{\partial W}$  with:

$$\frac{\partial E_t}{\partial W} = \frac{\partial E_t}{\partial W^r} + \mathbf{i} \frac{\partial E_t}{\partial W^i} + \mathbf{j} \frac{\partial E_t}{\partial W^j} + \mathbf{k} \frac{\partial E_t}{\partial W^k}. \quad (9)$$

Each term of the above relation is then computed by applying the chain rule. As a use-case for the equations, the mean squared error at a timestep  $t$  and named  $E_t$  is used as the loss function. Moreover, let  $\lambda$  be a fixed learning rate. First, the weight matrix  $W_{hy}$  is only seen in the equations of  $p_t$ . It is therefore straightforward to update each weight of  $W_{hy}$  at timestep  $t$  following:

$$W_{hy} = W_{hy} + \lambda \Delta_{hy}^t \otimes h_t^*, \quad (10)$$

with,

$$\Delta_{hy}^t = \frac{\partial E_t}{\partial W_{hy}} = (p_t - y_t). \quad (11)$$

Then, the weight matrices  $W_{hh}$  and  $W_{hx}$  are arguments of  $h_t$  with  $h_{t-1}$  involved. Therefore, the update equations are derived as:

$$W_{hh} = W_{hh} + \lambda \Delta_{hh}^t, \quad (12)$$

$$W_{hx} = W_{hx} + \lambda \Delta_{hx}^t, \quad (13)$$

with,

$$\Delta_{hh}^t = \frac{\partial E_t}{\partial W_{hh}} = \sum_{m=0}^t \left( \prod_{n=m}^t \delta_n \right) \otimes h_{m-1}^*, \quad (14)$$

$$\Delta_{hx}^t = \frac{\partial E_t}{\partial W_{hx}} = \sum_{m=0}^t \left( \prod_{n=m}^t \delta_n \right) \otimes x_m^*, \quad (15)$$

and,

$$\delta_n = \begin{cases} W_{hh}^* \otimes \delta_{n+1} \times \alpha'(h_n^{preact}) & \text{if } n \neq t \\ W_{hy}^* \otimes (p_n - y_n) \times \beta'(p_n^{preact}) & \text{else,} \end{cases} \quad (16)$$

With  $h_n^{preact}$  and  $p_n^{preact}$  the pre-activation values of  $h_n$  and  $p_n$  respectively. Finally, the biases are updated based on:

$$b_h = b_h + \lambda \Delta_{hh}^t. \quad (17)$$

### 2.4 Parameter initialization

A well-designed parameter initialization scheme strongly impacts on the efficiency of a DNN. An appropriate initialization, in fact, improves DNN convergence, reduces the risk of exploding or vanishing gradient, and often leads to a substantial performance improvement [11]. It has been shown that the backpropagation through time algorithm of RNNs is degraded by an inappropriate parameter initialization [32]. Moreover, an hyper-complex parameter cannot be simply initialized randomly and component-wise, due to the interactions between components. Therefore, this section proposes a procedure reported in Algorithm 1 to initialize a matrix  $W$  of quaternion-valued weights following four steps. The proposed initialization equations are derived from the polar form of a weight  $w$  of  $W$ :

$$w = |w| e^{q_{imag}^\triangle \theta} = |w| (\cos(\theta) + q_{imag}^\triangle \sin(\theta)), \quad (18)$$

and,

$$\begin{aligned} w_{\mathbf{r}} &= \varphi \cos(\theta), \\ w_{\mathbf{i}} &= \varphi q_{imagi}^\triangle \sin(\theta), \\ w_{\mathbf{j}} &= \varphi q_{imagj}^\triangle \sin(\theta), \\ w_{\mathbf{k}} &= \varphi q_{imagk}^\triangle \sin(\theta). \end{aligned} \quad (19)$$

---

**Algorithm 1** Quaternion-valued weight initialization

---

```

1: procedure QINIT( $W, n_{in}, n_{out}$ )
2:
3:    $\sigma \leftarrow \frac{1}{\sqrt{2(n_{in}+n_{out})}}$   $\triangleright$  w.r.t to Glorot criterion and eq. 23
4:
5:   for  $w$  in  $W$  do
6:      $\theta \leftarrow \text{rand}(-\pi, \pi)$ 
7:      $\varphi \leftarrow \text{rand}(-\sigma, \sigma)$ 
8:
9:      $x, y, z \leftarrow \text{rand}(0, 1)$ 
10:     $q_{imag} \leftarrow \text{Quaternion}(0, x, y, z)$ 
11:     $q_{imag}^\triangleleft \leftarrow \frac{q_{imag}}{\sqrt{x^2+y^2+z^2}}$ 
12:
13:     $w_r \leftarrow \varphi \times \cos(\theta)$   $\triangleright$  See eq. 19
14:     $w_i \leftarrow \varphi \times q_{imag}^\triangleleft \times \sin(\theta)$ 
15:     $w_j \leftarrow \varphi \times q_{imag}^\triangleleft \times \sin(\theta)$ 
16:     $w_k \leftarrow \varphi \times q_{imag}^\triangleleft \times \sin(\theta)$ 
17:     $w \leftarrow \text{Quaternion}(w_r, w_i, w_j, w_k)$ 

```

---

The angle  $\theta$  is randomly generated in the interval  $[-\pi, \pi]$ . The quaternion  $q_{imag}^\triangleleft$  is defined as purely normalized imaginary, and is expressed as  $q_{imag}^\triangleleft = 0 + xi + yj + zk$ . The imaginary components  $xi$ ,  $yi$ , and  $zk$  are sampled from an uniform distribution in  $[0, 1]$  to obtain  $q_{imag}$ , which is then normalized (following eq. 4) to obtain  $q_{imag}^\triangleleft$ . The parameter  $\varphi$  is a random number generated with respect to well-known initialization criterions (such as Glorot or He algorithms) [11, 12].

However, the equations derived in [11, 12] are defined for real-valued weight matrices. Therefore, the variance of  $W$  has to be investigated in the quaternion space to obtain  $\varphi$  (the full demonstration is provided in Appendix 5.1). The variance of  $W$  is defined as:

$$\text{Var}(W) = \mathbb{E}(|W|^2) - [\mathbb{E}(|W|)]^2, \quad (20)$$

with,

$$[\mathbb{E}(|W|)]^2 = 0. \quad (21)$$

Indeed, the weight distribution is symmetric around 0. The value of  $\text{Var}(W) = \mathbb{E}(|W|^2)$ , instead, is not trivial in the case of quaternion-valued matrices. Indeed,  $W$  follows a Chi-distribution with four degrees of freedom (DOFs). Consequently,  $\text{Var}(W)$  is expressed and computed as follows:

$$\text{Var}(W) = \mathbb{E}(|W|^2) = \int_0^\infty x^2 f(x) dx = 4\sigma^2. \quad (22)$$

The Glorot criterion [11] is thus extended to quaternion weight as following:

$$\sigma = \frac{1}{\sqrt{2(n_{in} + n_{out})}}, \quad (23)$$

with  $n_{in}$  and  $n_{out}$  the number of neurons of the input and output layers respectively. The He [12] criterion is derived in the same manner:

$$\sigma = \frac{1}{\sqrt{2n_{in}}}. \quad (24)$$

Finally,  $\varphi$  can be sampled from  $[-\sigma, \sigma]$  to complete the weight initialization of eq. 19.

### 3 Experiments

This section details the experimental setups and results obtained with QRNNs and RNNs on the copy task (Section 3.1), and on the TIMIT and Wall Street Journal (WSJ) speech recognition tasks (Section 3.2).

### 3.1 Copy task as a sanity check

The copy task originally introduced by [14] is a synthetic test that highlights long-term memory in models. This characteristic makes the copy task a powerful benchmark to demonstrate whether a recurrent model is able to learn long-term dependencies. It consists of binary input sequences of variable length  $L$ , followed by a sequence of blanks of size  $B$  and ended by a delimiter that announce the beginning of the copy operation (after which the initial input sequence should be progressively reconstructed at the output). In this paper, the copy-task is used as a sanity check to ensure that the introduction of quaternions does not harm the basic memorization abilities of RNNs. The RNNs and QRNNs used for the copy-task have an equal number of parameters (i.e., 0.3M) with only one hidden layer  $h$  of size 512 and 256 for RNN and QRNN, respectively. Moreover, only  $h$  is a quaternion dense layer since both inputs and outputs are real-valued. This alteration of the QRNN does not impact the value of the task as a sanity check. Indeed, long and short-term dependencies are captured within the hidden states that are quaternion-valued. Models are trained with the Adam optimizer, with an initial learning rate of  $\lambda = 3 \cdot 10^{-4}$ , and without employing any regularization methods. The training is stopped once the adopted binary cross-entropy loss function value drops down to 0.1 on the train set. The hidden activation function is linear, while the sigmoid is used as an output function. A set of 2,500 randomly generated sequences of length  $L = 20$  are used for training, while 10 random sequences of length  $L = 20$  are generated for evaluation.

Figure 1 shows the results achieved with RNNs and QRNNs on the described memory copy task. It is worth mentioning that both models converge to a loss of 0.1 with a final validation set accuracy of 0.98%. One can thus conclude that the introduction of quaternions in RNNs does not impact negatively on the ability of the hidden states to memorize previous time steps and BPTT to learn how to do that. Indeed, the testing reconstruction of the QRNN is nearly perfect.

### 3.2 Speech recognition

Experiments are performed with the TIMIT [10] phoneme recognition task, and the Wall Street Journal task (WSJ). Both benchmarks used quaternion acoustic features as input features, and are aligned with the Kaldi s5 recipes [26].

#### Quaternion acoustic features

The raw audio is first transformed into 40-dimensional log mel-filter-bank coefficients with first, second, and third order derivatives using the *pytorch-kaldi*<sup>3</sup> toolkit. An acoustic quaternion  $Q(f, t)$  associated with a frequency  $f$  and a time-frame  $t$  is formed as follows:

$$Q(f, t) = e(f, t) + \frac{\partial e(f, t)}{\partial t} \mathbf{i} + \frac{\partial^2 e(f, t)}{\partial^2 t} \mathbf{j} + \frac{\partial^3 e(f, t)}{\partial^3 t} \mathbf{k}. \quad (25)$$

$Q(f, t)$  represents multiple views of a frequency  $f$  at time frame  $t$ , consisting of the energy  $e(f, t)$  in the filter band at frequency  $f$ , its first time derivative describing a slope view, its second time derivative describing a concavity view, and the third derivative describing the rate of change of the second derivative. Thus, the quaternion input vector length is  $160/4 = 40$ . Decoding is based on Kaldi [26] and weighted finite state transducers (WFST) [19] that integrate acoustic, lexicon and language model probabilities into a single HMM-based search graph.

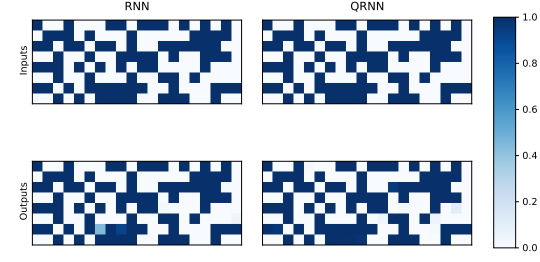


Figure 1: Experiment results on the synthetic copy task. The top row shows a random testing input sequence of binary vectors, while the bottom row presents the corresponding reconstructed sequences of RNN and QRNN.

Figure 1 shows the results achieved with RNNs and QRNNs on the described memory copy task. It is worth mentioning that both models converge to a loss of 0.1 with a final validation set accuracy of 0.98%. One can thus conclude that the introduction of quaternions in RNNs does not impact negatively on the ability of the hidden states to memorize previous time steps and BPTT to learn how to do that. Indeed, the testing reconstruction of the QRNN is nearly perfect.

#### Quaternion acoustic features

The raw audio is first transformed into 40-dimensional log mel-filter-bank coefficients with first, second, and third order derivatives using the *pytorch-kaldi*<sup>3</sup> toolkit. An acoustic quaternion  $Q(f, t)$  associated with a frequency  $f$  and a time-frame  $t$  is formed as follows:

$$Q(f, t) = e(f, t) + \frac{\partial e(f, t)}{\partial t} \mathbf{i} + \frac{\partial^2 e(f, t)}{\partial^2 t} \mathbf{j} + \frac{\partial^3 e(f, t)}{\partial^3 t} \mathbf{k}. \quad (25)$$

$Q(f, t)$  represents multiple views of a frequency  $f$  at time frame  $t$ , consisting of the energy  $e(f, t)$  in the filter band at frequency  $f$ , its first time derivative describing a slope view, its second time derivative describing a concavity view, and the third derivative describing the rate of change of the second derivative. Thus, the quaternion input vector length is  $160/4 = 40$ . Decoding is based on Kaldi [26] and weighted finite state transducers (WFST) [19] that integrate acoustic, lexicon and language model probabilities into a single HMM-based search graph.

<sup>3</sup><https://github.com/mravanelli/pytorch-kaldi>

## TIMIT

The training process is based on the standard 3,696 sentences uttered by 462 speakers, while test is conducted on 192 sentences uttered by 24 speakers. A validation set composed of 400 sentences uttered by 50 speakers is used for hyper-parameter tuning. QRNNs and RNNs are compared on two different TIMIT benchmarks. In the first one, the performance obtained by varying the number of hidden layers  $M$  (from 3 to 4) and neurons  $N$  (from 256 to 3,072) is investigated. However, it is worth underlying that the number of hidden neurons in the quaternion and real spaces do not handle the same amount of real-number values. Indeed, 256 quaternion neurons output are  $256 \times 4 = 1024$  real values. Therefore, for a fair comparison, the number of neurons is represented in the real-valued space (e.g., a number of real-valued neurons of 256 corresponds to  $256/4 = 64$  quaternion-valued neurons). Moreover, to compare both models with the same number of parameters, a second experiment is conducted considering 1M, 10M and 20M free parameters for both models. ReLU activations [20] are used across all the layers except for the output layer that is based on a softmax function. Models are optimized with Adam [16] with vanilla hyper-parameters and an initial learning rate of  $1 \cdot 10^{-4}$ . The learning rate is progressively annealed using an halving factor of 0.5 that is applied when no performance improvement on the validation set is observed. A dropout rate of 0.2 is applied over all the hidden layers [31]. The negative log-likelihood loss function is used as an objective function. All the experiments are repeated at least 3 times (3-folds) with different seeds and are averaged to limit any variation due to the random initialization.

Table 1: Phoneme error rate (PER%) of both QRNN and RNN models on the test set of the TIMIT dataset. “Params” stands for the total number of trainable parameters. The results are from a 3 folds average.

| # Layers | # Neurons | QRNN PER %  | RNN PER %   | QRNN Params  | RNN Params   |
|----------|-----------|-------------|-------------|--------------|--------------|
| 3        | 256       | 23.2        | 21.1        | 0.5M         | 0.8M         |
| 3        | 512       | 21.1        | 18.8        | 1.3M         | 2.8M         |
| 3        | 1024      | 18.5        | 17.7        | 3.3M         | 7.3M         |
| 3        | 2048      | 17.3        | 17.5        | 9.2M         | 25M          |
| 3        | 3072      | 17.4        | 17.7        | 17.6M        | 53.3M        |
| 4        | 256       | 23.7        | 21.2        | 0.6M         | 1M           |
| 4        | 512       | 20.9        | 18.7        | 1.4M         | 2.9M         |
| 4        | 1024      | 17.6        | 17.6        | 3.8M         | 9.4M         |
| 4        | 2048      | <b>17.0</b> | <b>17.3</b> | <b>11.3M</b> | <b>33.4M</b> |
| 4        | 3072      | 17.2        | 18.1        | 22.3M        | 72.1M        |

The results on the TIMIT task are reported in Table 1. The best PER is 17.0% and 17.3% for QRNN and RNN models respectively, highlighting an absolute improvement of 0.3% obtained with QRNN. These results compare favorably with the best results obtained so far with architectures that do not integrate access control in multiple memory layers [27]. Moreover, a remarkable advantage of QRNNs is a drastic reduction (with a factor of 3 $\times$ ) of the parameters needed to achieve these results. Indeed, such PERs are obtained with models that employ the same number of layers ( $L = 4$ ) and the same number of neurons ( $N = 2,048$ ), resulting in a number of parameters of 11.3M for QRNN against the 33.4M used in the real-valued RNN. It is also worth noting that QRNNs consistently need less parameters than equivalently sized RNNs, with an average reduction factor of 55.3%. This is easily explained by considering the content of quaternion algebra. Indeed, for a fully-connected layer with 2,048 input values and 2,048 hidden units, a real-valued RNN has  $2,048^2 \approx 4.2M$  parameters, while to maintain equal input and output dimensions the quaternion equivalent has 512 quaternions inputs and 512 quaternion hidden units. Therefore, the number of parameters for the quaternion-valued model is  $512^2 \times 4 \approx 1M$ . Such a complexity reduction turns out to produce better results and have other advantages such as a smaller memory footprint while saving NN models on budget memory systems. This characteristic makes our QRNN model particularly suitable for speech recognition conducted on low computational power devices like smartphones and tablets [6].

QRNNs and RNNs accuracies vary accordingly to the architecture with better PER on bigger and wider topologies. However, while QRNNs reach better performances with medium and large sized models, they perform worse than RNNs with few parameters. In particular, the worst PER are 23.7% and 21.1%, obtained with 0.5M and 0.8M parameters for the QRNN and the RNN, respectively. Such a difference is explained by a very small number of quater-

nion neurons in the hidden layers of these models, that might hinder learning proper representations. Indeed, the corresponding QRNN has 64 neurons only, compared to 256 for the RNN. Table 2 shows the results obtained with QRNNs and RNNs employing the same number of parameters. Consistently with our previous findings, QRNNs outperform RNNs when a sufficiently large model is trained. When considering 20 M parameters, a PER of 17.1% vs 17.5% is obtained, while a 17.4% vs 17.7% is achieved with 10 M parameters. Only when drastically reducing the number of parameters to 1M, the QRNN tends to perform poorly (leading to a PER of 22.5% compared to 20.9% obtained with the RNN). Overall, QRNNs are more effective than RNN at learning compact representations, especially when dealing with a sufficient number of neurons.

### Wall Street Journal

RNNs and QRNNs are trained on both the 14 hour subset ‘train-si84’ and the full 81 hour dataset of the Wall Street Journal (WSJ) corpus, and the ‘test-dev93’ development set is employed for validation. The best configurations for the QRNN and RNN observed during the phoneme recognition task on TIMIT (see Table 1) are selected to conduct the experiments on the WSJ automatic speech recognition task. Therefore, both QRNNs and RNNs are made of 4 hidden layers of size 2,048. All the hyper-parameters are the same that on the previous TIMIT experiments. Table 3 depicts the word error rate (WER) obtained on both tasks (WSJ14h and WSJ81h) with RNN and QRNN based models. QRNNs outperform RNNs in the two tasks with a WER of 8.25% compared to 8.51% on the 14 hour subset, and a WER of 7.22% against 7.65% on the full 81 hour set, representing improvements of 0.26 and 0.43 points for the 14 hour and the 81 hour set respectively. Moreover, the number of free parameters is still  $2.55 \times$  lower for the QRNN compared to the RNN, with 14.3M against 36.5M. The experiments demonstrate that the QRNN results scale well with more realistic and bigger datasets.

## 4 Conclusion

**Summary.** This paper proposes to process sequences of multidimensional features (such as acoustic data) with a novel quaternion recurrent neural network (QRNN). Three different experiments on the memory copy task and automatic speech recognition have shown that: 1) QRNNs are more effective to learn a compact representation by outperforming RNNs with 2 to 3 times less free parameters; 2) Fixing the number of parameters, QRNNs obtain better accuracies than RNNs (with a sufficiently large model); Therefore, our initial intuition that the quaternion algebra offers a better and more compact representation for multidimensional features, alongside with a better learning capability of feature internal dependencies through the *Hamilton product*, have been demonstrated.

**Limitations and Future Work.** QRNNs are based on straightforward recurrent neural networks that are not specifically designed to solve long or short term dependencies as LSTMs or GRUs. Therefore a future work will consist of the transposition of such dependencies concepts to well-adapted quaternion-based multiplicative gates. Another investigation will be to develop other multi-view features that contribute to decrease ambiguities in representing phonemes in the quaternion space.

**Acknowledgments.** The authors would like to acknowledge the founding support of Orkis, the computing support of Compute Canada and , NSERC, Samsung, IBM and CHIST-ERA/FRQ.

Table 2: Experiment results expressed in term of phoneme error rate (PER) percentage on the test set of the TIMIT phoneme recognition task. The results are from a 3 folds average.

| Params. | QRNN        | RNN         | Improv.     |
|---------|-------------|-------------|-------------|
| 1M      | 22.5        | 20.9        | +1.6        |
| 10M     | 17.4        | 17.7        | -0.3        |
| 20M     | <b>17.1</b> | <b>17.5</b> | <b>-0.4</b> |

Table 3: Experiment results expressed in term of word error rate (WER) percentage on the test set (test\_eval92) of the WSJ task. The results are from a 3 folds average.

| Models | WSJ 14h     | WSJ 81h     | Params       |
|--------|-------------|-------------|--------------|
| RNN    | 8.51        | 7.65        | 36.5M        |
| QRNN   | <b>8.25</b> | <b>7.22</b> | <b>14.3M</b> |

## References

- [1] Paolo Arena, Luigi Fortuna, Giovanni Muscato, and Maria Gabriella Xibilia. Multilayer perceptrons to approximate quaternion valued functions. *Neural Networks*, 10(2):335–342, 1997.
- [2] Paolo Arena, Luigi Fortuna, Luigi Occhipinti, and Maria Gabriella Xibilia. Neural networks for quaternion-valued function approximation. In *Circuits and Systems, ISCAS'94., IEEE International Symposium on*, volume 6, pages 307–310. IEEE, 1994.
- [3] Nicholas A Aspragathos and John K Dimitros. A comparative study of three methods for robot kinematics. *Systems, Man, and Cybernetics, Part B: Cybernetics, IEEE Transactions on*, 28(2):135–145, 1998.
- [4] Yoshua Bengio, Patrice Simard, and Paolo Frasconi. Learning long-term dependencies with gradient descent is difficult. *IEEE transactions on neural networks*, 5(2):157–166, 1994.
- [5] Anthony Maida Chase Gaudet. Deep quaternion networks. *arXiv preprint arXiv:1712.04604v2*, 2017.
- [6] G. Chen, C. Parada, and G. Heigold. Small-footprint keyword spotting using deep neural networks. In *2014 IEEE International Conference on Acoustics, Speech and Signal Processing (ICASSP)*, pages 4087–4091, May 2014.
- [7] Ivo Danihelka, Greg Wayne, Benigno Uria, Nal Kalchbrenner, and Alex Graves. Associative long short-term memory. *arXiv preprint arXiv:1602.03032*, 2016.
- [8] Steven B Davis and Paul Mermelstein. Comparison of parametric representations for monosyllabic word recognition in continuously spoken sentences. In *Readings in speech recognition*, pages 65–74. Elsevier, 1990.
- [9] Sadaoki Furui. Speaker-independent isolated word recognition based on emphasized spectral dynamics. In *Acoustics, Speech, and Signal Processing, IEEE International Conference on ICASSP'86.*, volume 11, pages 1991–1994. IEEE, 1986.
- [10] John S Garofolo, Lori F Lamel, William M Fisher, Jonathan G Fiscus, and David S Pallett. Darpa timit acoustic-phonetic continuous speech corpus cd-rom. nist speech disc 1-1.1. *NASA STI/Recon technical report n*, 93, 1993.
- [11] Xavier Glorot and Yoshua Bengio. Understanding the difficulty of training deep feedforward neural networks. In *International conference on artificial intelligence and statistics*, pages 249–256, 2010.
- [12] Kaiming He, Xiangyu Zhang, Shaoqing Ren, and Jian Sun. Delving deep into rectifiers: Surpassing human-level performance on imagenet classification. In *Proceedings of the IEEE international conference on computer vision*, pages 1026–1034, 2015.
- [13] Akira Hirose and Shotaro Yoshida. Generalization characteristics of complex-valued feedforward neural networks in relation to signal coherence. *IEEE Transactions on Neural Networks and learning systems*, 23(4):541–551, 2012.
- [14] Sepp Hochreiter and Jürgen Schmidhuber. Long short-term memory. *Neural computation*, 9(8):1735–1780, 1997.
- [15] Jin Hu and Jun Wang. Global stability of complex-valued recurrent neural networks with time-delays. *IEEE Transactions on Neural Networks and Learning Systems*, 23(6):853–865, 2012.
- [16] Diederik Kingma and Jimmy Ba. Adam: A method for stochastic optimization. *arXiv preprint arXiv:1412.6980*, 2014.
- [17] Larry R. Medsker and Lakhmi J. Jain. Recurrent neural networks. *Design and Applications*, 5, 2001.

[18] Toshifumi Minemoto, Teijiro Isokawa, Haruhiko Nishimura, and Nobuyuki Matsui. Feed forward neural network with random quaternionic neurons. *Signal Processing*, 136:59–68, 2017.

[19] Mehryar Mohri, Fernando Pereira, and Michael Riley. Weighted finite-state transducers in speech recognition. *Computer Speech and Language*, 16(1):69 – 88, 2002.

[20] Vinod Nair and Geoffrey E Hinton. Rectified linear units improve restricted boltzmann machines. In *Proceedings of the 27th International Conference on Machine Learning (ICML-10)*, pages 807–814, 2010.

[21] Tohru Nitta. A quaternary version of the back-propagation algorithm. In *Neural Networks, 1995. Proceedings., IEEE International Conference on*, volume 5, pages 2753–2756. IEEE, 1995.

[22] Titouan Parcollet, Mohamed Mochrid, Pierre-Michel Bousquet, Richard Dufour, Georges Linarès, and Renato De Mori. Quaternion neural networks for spoken language understanding. In *Spoken Language Technology Workshop (SLT), 2016 IEEE*, pages 362–368. IEEE, 2016.

[23] Titouan Parcollet, Mohamed Mochrid, and Georges Linares. Deep quaternion neural networks for spoken language understanding. In *Automatic Speech Recognition and Understanding Workshop (ASRU), 2017 IEEE*, pages 504–511. IEEE, 2017.

[24] Razvan Pascanu, Tomas Mikolov, and Yoshua Bengio. On the difficulty of training recurrent neural networks. In *International Conference on Machine Learning*, pages 1310–1318, 2013.

[25] Soo-Chang Pei and Ching-Min Cheng. Color image processing by using binary quaternion-moment-preserving thresholding technique. *IEEE Transactions on Image Processing*, 8(5):614–628, 1999.

[26] Daniel Povey, Arnab Ghoshal, Gilles Boulianne, Lukas Burget, Ondrej Glembek, Nagendra Goel, Mirko Hannemann, Petr Motlicek, Yanmin Qian, Petr Schwarz, Jan Silovsky, Georg Stemmer, and Karel Vesely. The kaldi speech recognition toolkit. In *IEEE 2011 Workshop on Automatic Speech Recognition and Understanding*. IEEE Signal Processing Society, December 2011. IEEE Catalog No.: CFP11SRW-USB.

[27] Mirco Ravanelli, Philemon Brakel, Maurizio Omologo, and Yoshua Bengio. Light gated recurrent units for speech recognition. *IEEE Transactions on Emerging Topics in Computational Intelligence*, 2(2):92–102, 2018.

[28] Sara Sabour, Nicholas Frosst, and Geoffrey E Hinton. Dynamic routing between capsules. *arXiv preprint arXiv:1710.09829v2*, 2017.

[29] Stephen John Sangwine. Fourier transforms of colour images using quaternion or hypercomplex, numbers. *Electronics letters*, 32(21):1979–1980, 1996.

[30] Jingyan Song and Yeung Yam. Complex recurrent neural network for computing the inverse and pseudo-inverse of the complex matrix. *Applied mathematics and computation*, 93(2-3):195–205, 1998.

[31] Nitish Srivastava, Geoffrey Hinton, Alex Krizhevsky, Ilya Sutskever, and Ruslan Salakhutdinov. Dropout: A simple way to prevent neural networks from overfitting. *The Journal of Machine Learning Research*, 15(1):1929–1958, 2014.

[32] Ilya Sutskever, James Martens, George Dahl, and Geoffrey Hinton. On the importance of initialization and momentum in deep learning. In *International conference on machine learning*, pages 1139–1147, 2013.

[33] Parcollet Titouan, Mohamed Mochrid, and Georges Linares. Quaternion denoising encoder-decoder for theme identification of telephone conversations. *Proc. Interspeech 2017*, pages 3325–3328, 2017.

[34] Chiheb Trabelsi, Olexa Bilaniuk, Dmitriy Serdyuk, Sandeep Subramanian, João Felipe Santos, Soroush Mehri, Negar Rostamzadeh, Yoshua Bengio, and Christopher J Pal. Deep complex networks. *arXiv preprint arXiv:1705.09792*, 2017.

- [35] Mark Tygert, Joan Bruna, Soumith Chintala, Yann LeCun, Serkan Piantino, and Arthur Szlam. A mathematical motivation for complex-valued convolutional networks. *Neural computation*, 28(5):815–825, 2016.
- [36] Scott Wisdom, Thomas Powers, John Hershey, Jonathan Le Roux, and Les Atlas. Full-capacity unitary recurrent neural networks. In *Advances in Neural Information Processing Systems*, pages 4880–4888, 2016.
- [37] D Xu, L Zhang, and H Zhang. Learning algorithms in quaternion neural networks using ghr calculus. *Neural Network World*, 27(3):271, 2017.

## 5 Appendix

### 5.1 Parameters initialization

Let us recall that a generated quaternion weight  $w$  from a weight matrix  $W$  has a polar form defined as:

$$w = |w|e^{q_{imag}^\triangleleft \theta} = |w|(\cos(\theta) + q_{imag}^\triangleleft \sin(\theta)), \quad (26)$$

with  $q_{imag}^\triangleleft = 0 + x\mathbf{i} + y\mathbf{j} + z\mathbf{k}$  a purely imaginary and normalized quaternion. Therefore,  $w$  can be computed following:

$$\begin{aligned} w_{\mathbf{r}} &= \varphi \cos(\theta), \\ w_{\mathbf{i}} &= \varphi q_{imag}^\triangleleft \sin(\theta), \\ w_{\mathbf{j}} &= \varphi q_{imag}^\triangleleft \sin(\theta), \\ w_{\mathbf{k}} &= \varphi q_{imag}^\triangleleft \sin(\theta). \end{aligned} \quad (27)$$

However,  $\varphi$  represents a randomly generated variable with respect to the variance of the quaternion weight and the selected initialization criterion. The initialization process follows [11] and [12] to derive the variance of the quaternion-valued weight parameters. Indeed, the variance of  $\mathbf{W}$  has to be investigated:

$$Var(W) = \mathbb{E}(|W|^2) - [\mathbb{E}(|W|)]^2. \quad (28)$$

$[\mathbb{E}(|W|)]^2$  is equals to 0 since the weight distribution is symmetric around 0. Nonetheless, the value of  $Var(W) = \mathbb{E}(|W|^2)$  is not trivial in the case of quaternion-valued matrices. Indeed,  $W$  follows a Chi-distribution with four degrees of freedom (DOFs) and  $\mathbb{E}(|W|^2)$  is expressed and computed as follows:

$$\mathbb{E}(|W|^2) = \int_0^\infty x^2 f(x) dx, \quad (29)$$

With  $f(x)$  is the probability density function with four DOFs. A four-dimensional vector  $X = \{A, B, C, D\}$  is considered to evaluate the density function  $f(x)$ .  $X$  has components that are normally distributed, centered at zero, and independents. Then,  $A, B, C$  and  $D$  have density functions:

$$f_A(x; \sigma) = f_B(x; \sigma) = f_C(x; \sigma) = f_D(x; \sigma) = \frac{e^{-x^2/2\sigma^2}}{\sqrt{2\pi\sigma^2}}. \quad (30)$$

The four-dimensional vector  $X$  has a length  $L$  defined as  $L = \sqrt{A^2 + B^2 + C^2 + D^2}$  with a cumulative distribution function  $F_L(x; \sigma)$  in the 4-sphere (n-sphere with  $n = 4$ )  $S_x$ :

$$F_L(x; \sigma) = \int \int \int \int_{S_x} f_A(x; \sigma) f_B(x; \sigma) f_C(x; \sigma) f_D(x; \sigma) dS_x \quad (31)$$

where  $S_x = \{(a, b, c, d) : \sqrt{a^2 + b^2 + c^2 + d^2} < x\}$  and  $dS_x = da db dc dd$ . The mere polar representations of the coordinates of  $X$  in a 4-dimensional space are defined to compute  $dS_x$ :

$$\begin{aligned} a &= \rho \cos \theta, \\ b &= \rho \sin \theta \cos \phi, \\ c &= \rho \sin \theta \sin \phi \cos \psi, \\ d &= \rho \sin \theta \sin \phi \sin \psi, \end{aligned}$$

where  $\rho$  is the magnitude ( $\rho = \sqrt{a^2 + b^2 + c^2 + d^2}$ ) and  $\theta, \phi$ , and  $\psi$  are the phases with  $0 \leq \theta \leq \pi$ ,  $0 \leq \phi \leq \pi$  and  $0 \leq \psi \leq 2\pi$ . Then,  $dS_x$  is evaluated with the Jacobian  $J_f$  of  $f$  defined as:

$$J_f = \frac{\partial(a, b, c, d)}{\partial(\rho, \theta, \phi, \psi)} = \frac{da db dc dd}{d\rho d\theta d\phi d\psi} = \begin{vmatrix} \frac{da}{d\rho} & \frac{da}{d\theta} & \frac{da}{d\phi} & \frac{da}{d\psi} \\ \frac{db}{d\rho} & \frac{db}{d\theta} & \frac{db}{d\phi} & \frac{db}{d\psi} \\ \frac{dc}{d\rho} & \frac{dc}{d\theta} & \frac{dc}{d\phi} & \frac{dc}{d\psi} \\ \frac{dd}{d\rho} & \frac{dd}{d\theta} & \frac{dd}{d\phi} & \frac{dd}{d\psi} \end{vmatrix}$$

$$= \begin{vmatrix} \cos \theta & -\rho \sin \theta & 0 & 0 \\ \sin \theta \cos \phi & \rho \sin \theta \cos \phi & -\rho \sin \theta \sin \phi & 0 \\ \sin \theta \sin \phi \cos \psi & \rho \cos \theta \sin \phi \cos \psi & \rho \sin \theta \cos \phi \cos \psi & -\rho \sin \theta \sin \phi \sin \psi \\ \sin \theta \sin \phi \sin \psi & \rho \cos \theta \sin \phi \sin \psi & \rho \sin \theta \cos \phi \sin \psi & \rho \sin \theta \sin \phi \cos \psi \end{vmatrix}.$$

And,

$$J_f = \rho^3 \sin^2 \theta \sin \phi. \quad (32)$$

Therefore, by the Jacobian  $J_f$ , we have the polar form:

$$da db dc dd = \rho^3 \sin^2 \theta \sin \phi d\rho d\theta d\phi d\psi. \quad (33)$$

Then, writing Eq.(31) in polar coordinates, we obtain:

$$\begin{aligned} F_L(x, \sigma) &= \left( \frac{1}{\sqrt{2\pi\sigma^2}} \right)^4 \int \int \int \int_0^x e^{-a^2/2\sigma^2} e^{-b^2/2\sigma^2} e^{-c^2/2\sigma^2} e^{-d^2/2\sigma^2} dS_x \\ &= \frac{1}{4\pi^2\sigma^4} \int_0^{2\pi} \int_0^\pi \int_0^\pi \int_0^x e^{-\rho^2/2\sigma^2} \rho^3 \sin^2 \theta \sin \phi d\rho d\theta d\phi d\psi \\ &= \frac{1}{4\pi^2\sigma^4} \int_0^{2\pi} d\psi \int_0^\pi \sin \phi d\phi \int_0^\pi \sin^2 \theta d\theta \int_0^x \rho^3 e^{-\rho^2/2\sigma^2} d\rho \\ &= \frac{1}{4\pi^2\sigma^4} 2\pi 2 \left[ \frac{\theta}{2} - \frac{\sin 2\theta}{4} \right]_0^\pi \int_0^x \rho^3 e^{-\rho^2/2\sigma^2} d\rho \\ &= \frac{1}{4\pi^2\sigma^4} 4\pi \frac{\pi}{2} \int_0^x \rho^3 e^{-\rho^2/2\sigma^2} d\rho, \end{aligned}$$

Then,

$$F_L(x, \sigma) = \frac{1}{2\sigma^4} \int_0^x \rho^3 e^{-\rho^2/2\sigma^2} d\rho. \quad (34)$$

The probability density function for  $X$  is the derivative of its cumulative distribution function, which by the fundamental theorem of calculus is:

$$\begin{aligned} f_L(x, \sigma) &= \frac{d}{dx} F_L(x, \sigma) \\ &= \frac{1}{2\sigma^4} x^3 e^{-x^2/2\sigma^2}. \end{aligned} \quad (35)$$

The expectation of the squared magnitude becomes:

$$\begin{aligned} \mathbb{E}(|W|^2) &= \int_0^\infty x^2 f(x) dx \\ &= \int_0^\infty x^2 \frac{1}{2\sigma^4} x^3 e^{-x^2/2\sigma^2} dx \\ &= \frac{1}{2\sigma^4} \int_0^\infty x^5 e^{-x^2/2\sigma^2} dx. \end{aligned}$$

With integration by parts we obtain:

$$\begin{aligned} \mathbb{E}(|W|^2) &= \frac{1}{2\sigma^4} \left( -x^4 \sigma^2 e^{-x^2/2\sigma^2} \Big|_0^\infty + \int_0^\infty \sigma^2 4x^3 e^{-x^2/2\sigma^2} dx \right) \\ &= \frac{1}{2\sigma^2} \left( -x^4 e^{-x^2/2\sigma^2} \Big|_0^\infty + \int_0^\infty 4x^3 e^{-x^2/2\sigma^2} dx \right). \end{aligned} \quad (36)$$

The expectation  $\mathbb{E}(|W|^2)$  is the sum of two terms. The first one:

$$\begin{aligned} -x^4 e^{-x^2/2\sigma^2} \Big|_0^\infty &= \lim_{x \rightarrow +\infty} -x^4 e^{-x^2/2\sigma^2} - \lim_{x \rightarrow 0} x^4 e^{-x^2/2\sigma^2} \\ &= \lim_{x \rightarrow +\infty} -x^4 e^{-x^2/2\sigma^2}, \end{aligned}$$

Based on the L'Hôpital's rule, the undetermined limit becomes:

$$\begin{aligned} \lim_{x \rightarrow +\infty} -x^4 e^{-x^2/2\sigma^2} &= -\lim_{x \rightarrow +\infty} \frac{x^4}{e^{x^2/2\sigma^2}} \\ &= \dots \\ &= -\lim_{x \rightarrow +\infty} \frac{24}{(1/\sigma^2)(P(x)e^{x^2/2\sigma^2})} \\ &= 0. \end{aligned} \tag{37}$$

With  $P(x)$  is polynomial and has a limit to  $+\infty$ . The second term is calculated in a same way (integration by parts) and  $\mathbb{E}(|W|^2)$  becomes from Eq.(36):

$$\begin{aligned} \mathbb{E}(|W|^2) &= \frac{1}{2\sigma^2} \int_0^\infty 4x^3 e^{-x^2/2\sigma^2} dx \\ &= \frac{2}{\sigma^2} \left( x^2 \sigma^2 e^{-x^2/2\sigma^2} \Big|_0^\infty + \int_0^\infty \sigma^2 2x e^{-x^2/2\sigma^2} dx \right). \end{aligned} \tag{38}$$

The limit of first term is equal to 0 with the same method than in Eq.(37). Therefore, the expectation is:

$$\begin{aligned} \mathbb{E}(|W|^2) &= 4 \left( \int_0^\infty x e^{-x^2/2\sigma^2} dx \right) \\ &= 4\sigma^2. \end{aligned} \tag{39}$$

And finally the variance is:

$$Var(|W|) = 4\sigma^2. \tag{40}$$

## 5.2 Quaternion backpropagation through time

Let us recall the forward equations and parameters needed to derive the complete quaternion backpropagation through time algorithm.

### Recall of the forward phase.

Let  $x_t$  be the input vector at timestep  $t$ ,  $h_t$  the hidden state,  $W_{hh}$ ,  $W_{xh}$  and  $W_{hy}$  the hidden state, input and output weight matrices respectively. Finally  $b_h$  is the biases vector of the hidden states and  $p_t, y_t$  are the output and the expected target vector.

$$h_t = \alpha(h_t^{preact}), \tag{41}$$

with,

$$h_t^{preact} = W_{hh} \otimes h_{t-1} + W_{xh} \otimes x_t + b_h, \tag{42}$$

and  $\alpha$  is the quaternion split activation function [37] of a quaternion  $Q$  defined as:

$$\alpha(Q) = f(r) + f(x)\mathbf{i} + f(y)\mathbf{j} + f(z)\mathbf{k}, \tag{43}$$

and  $f$  corresponding to any standard activation function. The output vector  $p_t$  can be computed as:

$$p_t = \beta(p_t^{preact}), \tag{44}$$

with

$$p_t^{preact} = W_{hy} \otimes h_t, \tag{45}$$

and  $\beta$  any split activation function. Finally, the objective function is a real-valued loss function applied component-wise. The gradient with respect to the MSE loss is expressed for each weight matrix as  $\frac{\partial E_t}{\partial W_{hy}}$ ,  $\frac{\partial E_t}{\partial W_{hh}}$ , and  $\frac{\partial E_t}{\partial W_{hx}}$ .

#### Output weight matrix.

The weight matrix  $W_{hy}$  is used only in the computation of  $p_t$ . It is therefore straightforward to compute  $\frac{\partial E_t}{\partial W_{hy}}$ :

$$\frac{\partial E_t}{\partial W_{hy}} = \frac{\partial E_t}{\partial W_{hy}^r} + i \frac{\partial E_t}{\partial W_{hy}^i} + j \frac{\partial E_t}{\partial W_{hy}^j} + k \frac{\partial E_t}{\partial W_{hy}^k}. \quad (46)$$

Each quaternion component is then derived following the chain rule:

$$\begin{aligned} \frac{\partial E_t}{\partial W_{hy}^r} &= \frac{\partial E_t}{\partial p_t^r} \frac{\partial p_t^r}{\partial W_{hy}^r} + \frac{\partial E_t}{\partial p_t^i} \frac{\partial p_t^i}{\partial W_{hy}^r} + \frac{\partial E_t}{\partial p_t^j} \frac{\partial p_t^j}{\partial W_{hy}^r} + \frac{\partial E_t}{\partial p_t^k} \frac{\partial p_t^k}{\partial W_{hy}^r} \\ &= (p_t^r - y_t^r) \times h_t^r + (p_t^i - y_t^i) \times h_t^i + (p_t^j - y_t^j) \times h_t^j + (p_t^k - y_t^k) \times h_t^k. \end{aligned} \quad (47)$$

$$\begin{aligned} \frac{\partial E_t}{\partial W_{hy}^i} &= \frac{\partial E_t}{\partial p_t^r} \frac{\partial p_t^r}{\partial W_{hy}^i} + \frac{\partial E_t}{\partial p_t^i} \frac{\partial p_t^i}{\partial W_{hy}^i} + \frac{\partial E_t}{\partial p_t^j} \frac{\partial p_t^j}{\partial W_{hy}^i} + \frac{\partial E_t}{\partial p_t^k} \frac{\partial p_t^k}{\partial W_{hy}^i} \\ &= (p_t^r - y_t^r) \times -h_t^i + (p_t^i - y_t^i) \times h_t^r + (p_t^j - y_t^j) \times h_t^k + (p_t^k - y_t^k) \times -h_t^j. \end{aligned} \quad (48)$$

$$\begin{aligned} \frac{\partial E_t}{\partial W_{hy}^j} &= \frac{\partial E_t}{\partial p_t^r} \frac{\partial p_t^r}{\partial W_{hy}^j} + \frac{\partial E_t}{\partial p_t^i} \frac{\partial p_t^i}{\partial W_{hy}^j} + \frac{\partial E_t}{\partial p_t^j} \frac{\partial p_t^j}{\partial W_{hy}^j} + \frac{\partial E_t}{\partial p_t^k} \frac{\partial p_t^k}{\partial W_{hy}^j} \\ &= (p_t^r - y_t^r) \times -h_t^j + (p_t^i - y_t^i) \times -h_t^k + (p_t^j - y_t^j) \times h_t^r + (p_t^k - y_t^k) \times h_t^i. \end{aligned} \quad (49)$$

$$\begin{aligned} \frac{\partial E_t}{\partial W_{hy}^k} &= \frac{\partial E_t}{\partial p_t^r} \frac{\partial p_t^r}{\partial W_{hy}^k} + \frac{\partial E_t}{\partial p_t^i} \frac{\partial p_t^i}{\partial W_{hy}^k} + \frac{\partial E_t}{\partial p_t^j} \frac{\partial p_t^j}{\partial W_{hy}^k} + \frac{\partial E_t}{\partial p_t^k} \frac{\partial p_t^k}{\partial W_{hy}^k} \\ &= (p_t^r - y_t^r) \times -h_t^k + (p_t^i - y_t^i) \times h_t^j + (p_t^j - y_t^j) \times -h_t^i + (p_t^k - y_t^k) \times h_t^r. \end{aligned} \quad (50)$$

By regrouping in a matrix form the  $h_t$  components from these equations, one can defines:

$$\begin{bmatrix} h_t^r & h_t^i & h_t^j & h_t^k \\ -h_t^i & h_t^r & h_t^k & -h_t^j \\ -h_t^j & -h_t^k & h_t^r & h_t^i \\ -h_t^k & h_t^j & -h_t^i & h_t^r \end{bmatrix} = h_t^*. \quad (51)$$

Therefore,

$$\frac{\partial E_t}{\partial W_{hy}} = (p_t - y_t) \otimes h_t^*. \quad (52)$$

#### Hidden weight matrix.

Conversely to  $W_{hy}$  the weight matrix  $W_{hh}$  is an argument of  $h_t$  with  $h_{t-1}$  involved. The recursive backpropagation can thus be derived as:

$$\frac{\partial E}{\partial W_{hh}} = \sum_{t=0}^N \frac{\partial E_t}{\partial W_{hh}}. \quad (53)$$

And,

$$\frac{\partial E_t}{\partial W_{hh}} = \sum_{m=0}^t \frac{\partial E_m}{\partial W_{hh}^r} + i \frac{\partial E_m}{\partial W_{hh}^i} + j \frac{\partial E_m}{\partial W_{hh}^j} + k \frac{\partial E_m}{\partial W_{hh}^k}. \quad (54)$$

As for  $W_{hy}$  we start with  $\frac{\partial E_k}{\partial W_{hh}^r}$ :

$$\begin{aligned} \sum_{m=0}^t \frac{\partial E_m}{\partial W_{hh}^r} &= \sum_{m=0}^t \frac{\partial E_t}{\partial h_t^r} \frac{\partial h_t^r}{\partial h_m^r} \frac{\partial h_m^r}{\partial W_{hh}^r} + \frac{\partial E_t}{\partial h_t^i} \frac{\partial h_t^i}{\partial h_m^i} \frac{\partial h_m^i}{\partial W_{hh}^r} \\ &\quad + \frac{\partial E_t}{\partial h_t^j} \frac{\partial h_t^j}{\partial h_m^j} \frac{\partial h_m^j}{\partial W_{hh}^r} + \frac{\partial E_t}{\partial h_t^k} \frac{\partial h_t^k}{\partial h_m^k} \frac{\partial h_m^k}{\partial W_{hh}^r}. \end{aligned} \quad (55)$$

Non-recursive elements are derived w.r.t  $r, i, j, k$ :

$$\begin{aligned}\frac{\partial E_t}{\partial h_t^r} &= \frac{\partial E_t}{\partial p_t^r} \frac{\partial p_t^r}{\partial h_t^r} + \frac{\partial E_t}{\partial p_t^i} \frac{\partial p_t^i}{\partial h_t^r} + \frac{\partial E_t}{\partial p_t^j} \frac{\partial p_t^j}{\partial h_t^r} + \frac{\partial E_t}{\partial p_t^k} \frac{\partial p_t^k}{\partial h_t^r} \\ &= (p_t^r - y_t^r) \times f'(p_t^r) \times W_{hy}^r + (p_t^i - y_t^i) \times f'(p_t^i) \times W_{hy}^i \\ &\quad + (p_t^j - y_t^j) \times f'(p_t^j) \times W_{hy}^j + (p_t^k - y_t^k) \times f'(p_t^k) \times W_{hy}^k.\end{aligned}\tag{56}$$

$$\begin{aligned}\frac{\partial E_t}{\partial h_t^i} &= \frac{\partial E_t}{\partial p_t^r} \frac{\partial p_t^r}{\partial h_t^i} + \frac{\partial E_t}{\partial p_t^i} \frac{\partial p_t^i}{\partial h_t^i} + \frac{\partial E_t}{\partial p_t^j} \frac{\partial p_t^j}{\partial h_t^i} + \frac{\partial E_t}{\partial p_t^k} \frac{\partial p_t^k}{\partial h_t^i} \\ &= (p_t^r - y_t^r) \times f'(p_t^r) \times -W_{hy}^i + (p_t^i - y_t^i) \times f'(p_t^i) \times W_{hy}^r \\ &\quad + (p_t^j - y_t^j) \times f'(p_t^j) \times W_{hy}^k + (p_t^k - y_t^k) \times f'(p_t^k) \times -W_{hy}^j.\end{aligned}\tag{57}$$

$$\begin{aligned}\frac{\partial E_t}{\partial h_t^j} &= \frac{\partial E_t}{\partial p_t^r} \frac{\partial p_t^r}{\partial h_t^j} + \frac{\partial E_t}{\partial p_t^i} \frac{\partial p_t^i}{\partial h_t^j} + \frac{\partial E_t}{\partial p_t^j} \frac{\partial p_t^j}{\partial h_t^j} + \frac{\partial E_t}{\partial p_t^k} \frac{\partial p_t^k}{\partial h_t^j} \\ &= (p_t^r - y_t^r) \times f'(p_t^r) \times -W_{hy}^j + (p_t^i - y_t^i) \times f'(p_t^i) \times -W_{hy}^k \\ &\quad + (p_t^j - y_t^j) \times f'(p_t^j) \times W_{hy}^r + (p_t^k - y_t^k) \times f'(p_t^k) \times W_{hy}^i.\end{aligned}\tag{58}$$

$$\begin{aligned}\frac{\partial E_t}{\partial h_t^k} &= \frac{\partial E_t}{\partial p_t^r} \frac{\partial p_t^r}{\partial h_t^k} + \frac{\partial E_t}{\partial p_t^i} \frac{\partial p_t^i}{\partial h_t^k} + \frac{\partial E_t}{\partial p_t^j} \frac{\partial p_t^j}{\partial h_t^k} + \frac{\partial E_t}{\partial p_t^k} \frac{\partial p_t^k}{\partial h_t^k} \\ &= (p_t^r - y_t^r) \times f'(p_t^r) \times -W_{hy}^k + (p_t^i - y_t^i) \times f'(p_t^i) \times W_{hy}^j \\ &\quad + (p_t^j - y_t^j) \times f'(p_t^j) \times -W_{hy}^i + (p_t^k - y_t^k) \times f'(p_t^k) \times W_{hy}^r.\end{aligned}\tag{59}$$

Then,

$$\frac{\partial h_{r,m}}{\partial W_{hh}^r} = h_{r,t-1}.\tag{60}$$

$$\frac{\partial h_{i,m}}{\partial W_{hh}^r} = h_{i,t-1}.\tag{61}$$

$$\frac{\partial h_{j,m}}{\partial W_{hh}^r} = h_{j,t-1}.\tag{62}$$

$$\frac{\partial h_{k,m}}{\partial W_{hh}^r} = h_{k,t-1}.\tag{63}$$

The remaining terms  $\frac{\partial h_t^r}{\partial h_m^r}, \frac{\partial h_t^i}{\partial h_m^i}, \frac{\partial h_t^j}{\partial h_m^j}$  and  $\frac{\partial h_t^k}{\partial h_m^k}$  are recursive and are written as:

$$\begin{aligned}\frac{\partial h_{r,t}}{\partial h_{r,m}} &= \prod_{n=m+1}^t \frac{\partial h_{r,n}}{\partial h_{r,n}^{preact}} \frac{\partial h_{r,n}^{preact}}{\partial h_{r,n-1}} + \frac{\partial h_{r,n}}{\partial h_{i,n}^{preact}} \frac{\partial h_{i,n}^{preact}}{\partial h_{r,n-1}} \\ &\quad + \frac{\partial h_{r,n}}{\partial h_{j,n}^{preact}} \frac{\partial h_{j,n}^{preact}}{\partial h_{r,n-1}} + \frac{\partial h_{r,n}}{\partial h_{k,n}^{preact}} \frac{\partial h_{k,n}^{preact}}{\partial h_{r,n-1}},\end{aligned}\tag{64}$$

simplified with,

$$\begin{aligned}\frac{\partial h_{r,t}}{\partial h_{r,m}} &= \prod_{n=m+1}^t \frac{\partial h_{r,n}}{\partial h_{r,n}^{preact}} \times W_{hh}^r + \frac{\partial h_{r,n}}{\partial h_{i,n}^{preact}} \times W_{hh}^i \\ &\quad + \frac{\partial h_{r,n}}{\partial h_{j,n}^{preact}} \times W_{hh}^j + \frac{\partial h_{r,n}}{\partial h_{k,n}^{preact}} \times W_{hh}^k.\end{aligned}\tag{65}$$

Consequently,

$$\begin{aligned} \frac{\partial h_{i,t}}{\partial h_{i,m}} &= \prod_{n=m+1}^t \frac{\partial h_{i,n}}{\partial h_{r,n}^{preact}} \times -W_{hh}^i + \frac{\partial h_{i,n}}{\partial h_{i,n}^{preact}} \times W_{hh}^r \\ &\quad + \frac{\partial h_{j,n}}{\partial h_{j,n}^{preact}} \times W_{hh}^k + \frac{\partial h_{i,n}}{\partial h_{k,n}^{preact}} \times -W_{hh}^j. \end{aligned} \quad (66)$$

$$\begin{aligned} \frac{\partial h_{j,t}}{\partial h_{j,m}} &= \prod_{n=m+1}^t \frac{\partial h_{j,n}}{\partial h_{r,n}^{preact}} \times -W_{hh}^j + \frac{\partial h_{j,n}}{\partial h_{i,n}^{preact}} \times -W_{hh}^k \\ &\quad + \frac{\partial h_{j,n}}{\partial h_{j,n}^{preact}} \times W_{hh}^r + \frac{\partial h_{j,n}}{\partial h_{k,n}^{preact}} \times W_{hh}^i. \end{aligned} \quad (67)$$

$$\begin{aligned} \frac{\partial h_{k,t}}{\partial h_{k,m}} &= \prod_{n=m+1}^t \frac{\partial h_{k,n}}{\partial h_{r,n}^{preact}} \times -W_{hh}^k + \frac{\partial h_{k,n}}{\partial h_{i,n}^{preact}} \times W_{hh}^j \\ &\quad + \frac{\partial h_{k,n}}{\partial h_{j,n}^{preact}} \times -W_{hh}^i + \frac{\partial h_{k,n}}{\partial h_{k,n}^{preact}} \times W_{hh}^r. \end{aligned} \quad (68)$$

The same operations are performed for  $\mathbf{i}, \mathbf{j}, \mathbf{k}$  in eq. 72 and  $\frac{\partial E_t}{\partial W_{hh}}$  can finally be expressed as:

$$\frac{\partial E_t}{\partial W_{hh}} = \sum_{m=0}^t \left( \prod_{n=m+1}^t \delta_n \right) \otimes h_{t-1}^*, \quad (69)$$

with,

$$\delta_n = \begin{cases} W_{hh}^* \otimes \delta_{n+1} \times \alpha'(h_n^{preact}) & \text{if } n \neq t \\ W_{hy}^* \otimes (p_n - y_n) \times \beta'(p_n^{preact}) & \text{else.} \end{cases} \quad (70)$$

### Input weight matrix.

$\frac{\partial E_t}{\partial W_{hx}}$  is computed in the exact same manner as  $\frac{\partial E_t}{\partial W_{hh}}$ .

$$\frac{\partial E}{\partial W_{hx}} = \sum_{t=0}^N \frac{\partial E_t}{\partial W_{hx}}. \quad (71)$$

And,

$$\frac{\partial E_t}{\partial W_{hx}} = \sum_{m=0}^t \frac{\partial E_m}{\partial W_{hx}^r} + i \frac{\partial E_m}{\partial W_{hx}^r} + j \frac{\partial E_m}{\partial W_{hx}^i} + k \frac{\partial E_m}{\partial W_{hx}^k}. \quad (72)$$

Therefore  $\frac{\partial E_t}{\partial W_{hx}}$  is easily extend as:

$$\frac{\partial E_t}{\partial W_{hx}} = \sum_{m=0}^t \left( \prod_{n=m+1}^t \delta_n \right) \otimes x_t^*. \quad (73)$$